Exelon Generation
4300 Winfield Road
Warrenville, IL 60555

www.exeloncorp.com

Exelon Nuclear

10 CFR 50.55a

RS-07-059

May 3, 2007

U. S. Nuclear Regulatory Commission
ATTN: Document Control Desk
Washington, DC 20555-0001

Byron Station Unit 2
Facility Operating License No. NPF-66
NRC Docket No. STN 50-455

Subject: Transmittal of WCAP-16401-NP, Revision 0, "Technical Basis for Repair Options for Reactor Vessel Head Penetration Nozzles and Attachment Welds: Byron and Braidwood Units 1 and 2"

References: (1) Letter from D. M. Benyak (Exelon Generation Company, LLC) to U. S. NRC, "Byron Station Unit 2 Inservice Inspection Relief Request I3R-14: Alternative Requirements for the Repair of a Reactor Vessel Head Penetration," dated April 13, 2007

(2) Letter from D. M. Benyak (Exelon Generation Company, LLC) to U. S. NRC, "Supporting Information for Byron Station Unit 2 Inservice Inspection Relief Request I3R-14: Alternative Requirements for the Repair of a Reactor Vessel Head Penetration," dated April 13, 2007

The Reference (1) submittal proposed an alternative repair technique using the embedding methodology of Westinghouse WCAP-15987, Revision 2-A, "Technical Basis for the Embedded Flaw Process for Repair of Reactor Vessel Head Penetrations," and was supported by evaluations provided in WCAP-16401-P, Revision 0, "Technical Basis for Repair Options for Reactor Vessel Head Penetration Nozzles and Attachment Welds."

Reference (2) provided the proprietary version of the WCAP-16401 evaluation. The attachment provides the non-proprietary version (i.e., WCAP-16401-NP Revision 0) of this evaluation.

There are no regulatory commitments contained in this submittal. If you have any questions regarding this submittal, please contact Mr. David Chrzanowski at (630) 657-2816.

Respectfully,

Darin M Benyak

Darin M. Benyak
Director, Licensing and Regulatory Affairs

Attachment – Westinghouse WCAP-16401-NP, Revision 0, "Technical Basis for Repair Options for Reactor Vessel Head Penetration Nozzles and Attachment Welds: Byron and Braidwood Units 1 and 2" (Non-Proprietary)

Attachment

Westinghouse WCAP-16401-NP, Revision 0

Technical Basis for Repair Options for Reactor Vessel Head Penetration Nozzles and Attachment Welds

Byron and Braidwood Units 1 and 2
(Non-Proprietary)

Westinghouse Non-Proprietary Class 3

WCAP-16401-NP
Revision 0

April 2007

Technical Basis for Repair Options for Reactor Vessel Head Penetration Nozzles and Attachment Welds: Byron and Braidwood Units 1 and 2

WCAP-16401-NP
Revision 0

Technical Basis for Repair Options for Reactor Vessel Head Penetration Nozzles and Attachment Welds: Byron and Braidwood Units 1 and 2

A. Udyawar

April 2007

Verifier: C. Y. Yang*
Piping Analysis & Fracture Mechanics

Approved: S. A. Swamy*
Manager, Piping Analysis & Fracture Mechanics

** Electronically approved records are authenticated in the Electronic Document Management System.*

Westinghouse Electric Company LLC
P.O. Box 355
Pittsburgh, PA 15230-0355

© 2007 Westinghouse Electric Company LLC
All Rights Reserved

TABLE OF CONTENTS

1 INTRODUCTION 1-1
2 TECHNICAL BASIS FOR APPLICATION OF EMBEDDED FLAW REPAIR METHOD TO HEAD PENETRATION NOZZLES 2-1
2.1 Acceptance Criteria 2-1
2.1.1 Acceptance Criteria for Axial Flaws 2-1
2.1.2 Acceptance Criteria for Circumferential Flaws 2-2
2.2 Methodology 2-2
2.2.1 Geometry and Source of Data 2-3
2.2.2 Loading Conditions 2-3
2.2.3 Stress Intensity Factor 2-4
2.2.4 Allowable Flaw Size Determination 2-5
2.2.5 Fatigue Crack Growth Prediction 2-5
2.3 FRACTURE MECHANICS ANALYSIS RESULTS 2-6
2.3.1 Results for Allowable Flaw Sizes (Without Fatigue Crack Growth Adjustment) 2-6
2.3.2 Results for Allowable Flaw Sizes (With Fatigue Crack Growth Adjustment) 2-7
2.4 Summary 2-7
3 TECHNICAL BASIS FOR APPLICATION OF EMBEDDED FLAW REPAIR METHOD TO PENETRATION NOZZLE ATTACHMENT WELDS 3-1
3.1 Acceptance Criteria 3-1
3.1.1 Section XI Appendix K 3-1
3.1.2 Primary Stress Limits 3-2
3.2 Methodology 3-2
3.2.1 Geometry and Source of Data 3-2
3.2.2 Loading Conditions 3-3
3.2.3 Stress Intensity Factor 3-3
3.2.4 Material Properties 3-4
3.2.5 Applied J-Integral 3-5
3.2.6 Fatigue Crack Growth Prediction 3-6
3.3 FRACTURE MECHANICS ANALYSIS RESULTS 3-7
3.3.1 Results for Applied J-Integral and Material J-R Curves 3-7
3.3.2 Results for Fatigue Crack Growth into the Vessel Head 3-8
3.3.3 Results for Fatigue Crack Growth into the Repair Weld 3-8
3.4 Summary 3-8
4 TECHNICAL BASIS FOR "AS-EXCAVATED" REPAIRS 4-1
4.1 Introduction 4-1
4.2 Technical Approach and Acceptance Criteria 4-1
4.3 Evaluation Results for the "As-Excavated" Repairs 4-2
4.4 Summary 4-2
5 SUMMARY AND CONCLUSIONS 5-1
6 REFERENCES 6-1

LIST OF TABLES

Table 2-1	Summary of Reactor Vessel Transients for Byron and Braidwood Units 1 and 2	2-8
Table 3-1	Geometry of Byron and Braidwood Units 1 and 2 Head Penetration Attachment Welds (All dimensions in inches)	3-9
Table 3-2	Results of Applied J-integral and Material J-R Curve	3-10
Table 4-1	Key Dimensions of Head Penetration Nozzles	4-3
Table 4-2	Results of Structural Qualification for "As-Excavated" Repairs (Housing Penetration Wall Thickness Reduced to 0.375 inch)	4-3

LIST OF FIGURES

Figure 2-1 Geometry of a Typical Closure Head Penetration 2-10
Figure 2-2 Analytical Stress Cuts Taken from the Finite Element Model 2-11
Figure 2-3 Allowable Axial Flaw Sizes In Penetration Nozzle (Without Fatigue Crack Growth) [ ]^{a,c,e} 2-12
Figure 2-4 Allowable Circumferential Flaw Sizes In Penetration Nozzle (Without Fatigue Crack Growth) [ ]^{a,c,e} 2-13
Figure 2-5 Fatigue Crack Growth Prediction for Repaired Axial Flaws in the Penetration Nozzles (Uphill side) 2-14
Figure 2-6 Fatigue Crack Growth Prediction for Repaired Axial Flaws in the Penetration Nozzles (Downhill side) 2-15
Figure 2-7 Maximum Allowable Axial Flaw Sizes in the Repaired Penetration Nozzles for 20 Years Service Life 2-16
Figure 2-8 Fatigue Crack Growth Prediction for Repaired Circumferential Flaws in the Penetration Nozzles (Uphill side) 2-17
Figure 2-9 Fatigue Crack Growth Prediction for Repaired Circumferential Flaws in the Penetration Nozzles (Downhill side) 2-18
Figure 2-10 Maximum Allowable Circumferential Flaw Sizes in the Repaired Penetration Nozzles for 20 Years Service Life 2-19
Figure 3-1 Geometry and Terminology as Applied in [ ]^{a,c,e} 3-11
Figure 3-2 Comparison of the Slope of the Applied J-integral and Material J-R Curve (Governing Transient: Loss of Load) 3-12
Figure 3-3 Fatigue Crack Growth Prediction in the Reactor Vessel Head with Maximum Postulated Flaws in the Attachment Weld 3-13
Figure 3-4 Linearized Representation of Through-Wall Stress Distribution 3-14

1 INTRODUCTION

Leakage has been reported from the reactor vessel closure head penetration nozzles in a number of plants. This has led to requests for inspection of these regions. Inspections of the leaking penetrations indicate the presence of axial cracks that extend above and below the head penetration attachment welds. The cause of these axially oriented cracks has been determined to result from primary water stress corrosion cracking (PWSCC) that are driven by both steady state operating and residual stress. The residual stress is due to weld shrinkage and the offset geometry of the attachment weld that induces bending of the penetration nozzle. The bending also contributed to the penetration nozzle being ovalized over the attachment weld region.

As a part of the inspection and repair efforts associated with the head penetration inspection program for Byron and Braidwood Units 1 and 2, engineering evaluations were performed to support the Westinghouse embedded flaw repair method. [

]^{a,c,e} The methodology used is based on extensive analytical work completed to-date for the Westinghouse Owners Group (WOG), and a large collection of test data obtained under the sponsorship of Westinghouse, Babcock & Wilcox (B&W) and Combustion Engineering Owners groups (CEOG), as well as the Electric Power Research Institute (EPRI). The technical basis of the embedded flaw repair method is documented in WCAP-15987-P [1] and has been reviewed and accepted by the NRC. In the NRC Safety Evaluation that was incorporated in WCAP-15987-P, the NRC staff concluded that, subject to the specified conditions and limitations, the embedded flaw repair process described in WCAP-15987-P provides an acceptable level of quality and safety. The staff also concluded that WCAP-15987-P is acceptable for referencing in licensing applications.

Section XI of the ASME Code did not have a provision for welding over an existing flaw until the 1992 Edition. Those plants inspecting to an earlier edition of the Code would have to process relief requests to use the embedded flaw repair method, or update to the 1992 Edition of the Code. The repair and replacements rules of IWA-4000 in Section XI, starting with the 1992 Edition, allow weld repair over an existing flaw, provided that the flaw can be shown to be acceptable to the analytical requirements of Section XI. Engineering evaluations were performed and the results are presented in this report to provide the maximum flaw sizes that would satisfy the requirements in Section XI of the ASME Code [2] and be suitable to support the embedded flaw repair process.

Section XI repair rules allow the use of grinding to remove flaws, regardless of the edition of the Code. The only requirement is to ensure that the excavated region still meets the stress limits of the original construction code, which was Section III. Evaluations were performed and the results presented in this report address the effects of the local structural discontinuities resulting from the grinding operations performed to excavate flaws in the head penetration nozzles.

The purpose of this report is to provide plant-specific technical basis for the use of the embedded flaw repair method and to confirm that Byron and Braidwood Units 1 and Unit 2 meet the criteria for application of the embedded flaw repair process stated in Appendix C of WCAP-15987-P [1]. The results

presented in this report would enable the weld repair team to effectively determine the appropriate repair method.

In this report, the technical basis and evaluation results to support the use of the embedded flaw repair method for a flawed head penetration nozzle are provided in Section 2. The technical basis and evaluation results that support a similar application for a flawed head penetration attachment weld are provided in Section 3. Results of the evaluation providing a basis for grinding operations to excavate flaws in the head penetration nozzles are discussed in Section 4.

Note that there are several locations in this report where proprietary information has been identified and bracketed. For each of the bracketed locations, the reason for the proprietary classification is given, using a standardized system. The proprietary brackets are labeled with three different letters to provide this information and the explanation for each letter is given below:

a. The information reveals the distinguishing aspects of a process or component, structure, tool, method, etc., and the prevention of its use by Westinghouse's competitors, without license from Westinghouse, gives Westinghouse a competitive economic advantage.

c. The information, if used by a competitor, would reduce the competitor's expenditure of resources or improve the competitor's advantage in the design, manufacture, shipment, installation, assurance of quality, or licensing of a similar product.

e. The information reveals aspects of past, present, or future Westinghouse or customer funded development plans and programs of potential commercial value to Westinghouse.

2 TECHNICAL BASIS FOR APPLICATION OF EMBEDDED FLAW REPAIR METHOD TO HEAD PENETRATION NOZZLES

This section provides a discussion on the technical basis for the use of embedded flaw repair method for a flawed head penetration nozzle. [

]^{a,c,e}

Flaw evaluations for postulated planar flaws with various flaw sizes and shapes in the head penetration nozzles were performed. Based on the results of these evaluations, the largest flaw size that can be repaired using the embedded flaw repair method is determined.

2.1 Acceptance Criteria

The evaluation procedures and acceptance criteria for indications in austenitic piping are contained in paragraph IWB-3640 of ASME Section XI [2]. [

]^{a,c,e}

2.1.1 Acceptance Criteria for Axial Flaws

For axial flaws, the hoop stress at limit load, σ_h, is first determined by using the following expression:

$$\sigma_h = \frac{\sigma_f}{SF_m}\left[\frac{1-\left(\frac{a}{t}\right)}{1-\left(\frac{a}{t}\right)/M_2}\right] \qquad (2\text{-}1)$$

where M_2 is the bulging factor given by:

$$M_2 = \left[1+\left(\frac{1.61}{4R_m t}\right)\ell^2\right]^{1/2} \qquad (2\text{-}2)$$

and

σ_f = $\frac{\sigma_u + \sigma_y}{2}$ (Average of Ultimate and Yield Strengths)

σ_h = PR_m/t (Hoop Stress due to Pressure P)

ℓ = Total Flaw Length

a = Flaw Depth

R_m = Mean Radius of Penetration Nozzle

t = Wall Thickness of Penetration Nozzle

SF_m = Safety Factor for membrane stress
2.7 for Level A Service Loading
2.4 for Level B Service Loading
1.8 for Level C Service Loading
1.3 for Level D Service Loading

The limits of applicability of this equation are $a/t \leq 0.75$ and $\ell < \ell_{allow}$

$$\ell_{allow} = 1.58(R_m t)^{0.5}[(\sigma_f/\sigma_h)^2 - 1]^{0.5} \quad (2\text{-}3)$$

This limit ensures that surface flaws would remain below the critical size based on the plastic collapse condition if they should grow through the wall.

2.1.2 Acceptance Criteria for Circumferential Flaws

For circumferential flaws, the axial membrane stress is calculated from internal pressure and axial components of other loads on the penetration nozzle. The axial primary membrane stress at limit load under pure membrane loading, σ_m^c, is calculated by using the following equations:

$$\sigma_m^c = \sigma_f[1-(\frac{a\theta}{t\pi})-\frac{2\varphi}{\pi}] \quad (2\text{-}4)$$

and

$$\varphi = \arcsin[\frac{1}{2}\left(\frac{a}{t}\right)\sin\theta]$$

where:

θ = Half Flaw Angle

σ_f = $\frac{\sigma_u + \sigma_y}{2}$ (Average of Ultimate and Yield Strengths)

The allowable primary membrane stress, S_t, is given by

$$S_t = \frac{\sigma_m^c}{SF_m} \quad (2\text{-}5)$$

where:

SF_m = Safety Factor for membrane stress depends on Service Level, as defined in Section 2.1.1.

2.2 METHODOLOGY

The evaluation assumes that a flaw has been detected in a penetration nozzle and that the embedded flaw repair method is used to seal the flaw from further exposure to the primary water environment. The

evaluation began with the determination of an allowable flaw size based on the acceptance criteria described in Section 2.1 for a flaw postulated in the penetration nozzle. [

]^{a,c,e}

2.2.1 Geometry and Source of Data

There are many head penetration nozzles in the reactor vessel upper head. The dimensions of the penetration nozzles as well as the reactor vessel heads and the location of the nozzles are the same in all the Byron and Braidwood Units. The outermost penetration nozzles (penetrations 74-78) were selected for analysis because the stresses in the outermost penetration nozzles are in general more dominating. A schematic of a closure head penetration nozzle for a typical Westinghouse design plant is shown in Figure 2-1.

The dimensions of all the penetration nozzles are identical, with a 4.00 inch Outside Diameter (OD) and a wall thickness of 0.625 inches. The distributions of residual, transient thermal, and pressure stresses in the vessel head penetration nozzle were obtained from detailed three-dimensional elastic-plastic finite element analyses [3] for Byron and Braidwood Units 1 and 2. The through-wall stress distributions from the finite element analyses were used to determine the fatigue crack growth and the resulting allowable flaw size for the postulated flaw in the repaired penetration nozzles. [

]^{a,c,e} The finite element model with the selected stress cuts used in the evaluation is shown in Figure 2-2. The term "stress cut" is defined as an imaginary line or plane over which stress distribution is evaluated. The regions of the head penetration that have the highest stresses are the ones in the vicinity of the attachment weld (Cuts 1 and 2 in Figure 2-2) which are the potential locations for crack initiation.

2.2.2 Loading Conditions

Thermal Transient Selection for Maximum Allowable Flaw Size Determination

The requirement for evaluating a flaw using the rules of Section XI is that the governing transients be chosen from the normal/upset conditions as well as from the emergency/faulted conditions. This is necessary because, as discussed in Section 2.1, different safety margins are used for the normal, upset, emergency, and faulted conditions. A lower safety factor is used to reflect a lower probability of occurrence for the emergency/faulted conditions.

[

]^{a,c,e}

Thermal Transient Selection for Fatigue Crack Growth Prediction

[

]^{a,c,e} The thermal transients that occur in the upper head region

are relatively mild, because most of the water in the head region has already passed through the core. The flow in the upper head is low compared to other regions of the reactor vessel, which mutes the effects of the operating thermal transients. The thermal transients that occur in Byron and Braidwood Units 1 and 2 are shown in Table 2-1. [

]^{a,c,e}

2.2.3 Stress Intensity Factor

One of the key elements in a fracture mechanics evaluation is the determination of the crack driving force or stress intensity factor, K_I. This is based on the equations available in the literature.

Stress Intensity Factor for Surface Flaw

For a part-through wall flaw, the stress profile is approximated by a cubic polynomial as follows:

$$\sigma(x) = A_0 + A_1 x + A_2 x^2 + A_3 x^3$$

where:

x	=	The distance into the wall (inch)
σ	=	Stress perpendicular to the plane of the crack (ksi)
A_i	=	Coefficients of the cubic polynomial fit, i = 0, 1, 2, 3

[

]^{a,c,e}

[

]^{a,c,e}

2.2.4 Allowable Flaw Size Determination

Allowable flaw sizes for axial and circumferential flaws with various aspect ratios (flaw length/flaw depth) in a penetration nozzle are calculated in accordance with the acceptance criteria discussed in Section 2.1. The thermal transients that have the [ ]^{a,c,e} were considered in determining the allowable flaw sizes. It should be noted that these allowable flaw sizes must be adjusted to account for fatigue crack growth. Since the repaired flaws are embedded and sealed, they are not subjected to PWSCC and hence the only mechanism for sub-critical crack growth is fatigue. Adjustments to the allowable flaw sizes are based on the results from the fatigue crack growth evaluation described in Section 2.2.5.

2.2.5 Fatigue Crack Growth Prediction

The analysis procedure involves postulating various types of flaw in the penetration nozzle subject to a series of design loads. The applied loads include pressure, thermal transients and residual stresses. The governing thermal transients used for this evaluation are shown in Section 2.2.2. The cycles are distributed evenly over the entire plant design life. The stress intensity factor range, ΔK_I, which controls fatigue crack growth, depends on the geometry of the crack, its surrounding structure and the range of applied stresses in the region of the postulated crack. Once ΔK_I is calculated, the fatigue crack growth due to a particular stress cycle can be determined using a crack growth rate reference curve applicable to the material of the head penetration nozzle.

The fatigue crack growth rate (CGR) reference curve for nickel base alloys in air environment is based on the results reported in [6] and is shown below.

$$\frac{da}{dN} = CS_R \Delta K^n \tag{2-7}$$

$$C = 4.835\times10^{-14} + 1.622\times10^{-16}T - 1.490\times10^{-18}T^2 + 4.355\times10^{-21}T^3 \tag{2-8}$$

$$S_R = \left[1 - 0.82R\ \right]^{-2.2}$$

$$n = 4.1$$

where:

T = Average temperature of the transient (°C)

ΔK = Stress intensity factor range ($MPa\sqrt{m}$)

R = Stress Ratio (K_{min}/K_{max})

da/dN = Fatigue crack growth rate (meters / cycle)

The crack growth rate reference curve in air used in determining the fatigue crack growth into the repair weld Alloy 52 is not available. However, there are limited test data on Alloy 52 in PWR water environment and, based on these data, the crack growth rates for Alloy 52 and Alloy 600 were concluded to be the same in PWR water environment [6]. Therefore, the crack growth rate curve for Alloy 52 in air is assumed to be the same as that for Alloy 600 in air.

Once the incremental crack growth corresponding to a specific transient for a small time period is calculated, it is added to the original crack size, and the analysis continues to the next time period and/or thermal transient. The procedure is repeated in this manner until all the significant analytical thermal transients and cycles known to occur in a given period of operation have been analyzed.

2.3 FRACTURE MECHANICS ANALYSIS RESULTS

Axial and circumferential flaws found in a head penetration nozzle can be repaired using the embedded flaw repair method. A range of potential flaw sizes and shapes was investigated to thoroughly evaluate the use of embedded flaw repair.

2.3.1 Results for Allowable Flaw Sizes (Without Fatigue Crack Growth Adjustment)

Allowable Flaw Sizes for Axial Flaws

[

]^{a,c,e} The allowable flaw sizes for a maximum design pressure of 2.5 ksi can be obtained as shown in Figure 2-3 for postulated inside surface axial flaws with various aspect ratios (flaw length/flaw depth). The allowable flaw sizes determined this way for the inside surface axial flaws can also be [ ]^{a,c,e} It should be noted that the allowable flaw sizes determined from Figure 2-3 must be adjusted to account for the fatigue crack growth of the repaired flaws, which are no longer subjected to stress corrosion cracking. The amount of adjustments is described in Section 2.3.2.

Allowable Flaw Sizes for Circumferential Flaws

[

]^{a,c,e} The allowable flaw sizes for a maximum design pressure of 2.5 ksi can be determined as shown in Figure 2-4 for postulated inside surface circumferential flaws with various aspect ratio (flaw length/flaw depth). The allowable flaw sizes determined this way for the inside surface flaws can also be [ ]^{a,c,e} It should be noted that the allowable flaw sizes determined from Figure 2-4 must be adjusted to account for the fatigue crack growth of the repaired flaws, which are no longer subjected to stress corrosion cracking. The amount of adjustments is described in Section 2.3.2.

2.3.2 Results for Allowable Flaw Sizes (With Fatigue Crack Growth Adjustment)

Fatigue crack growth (FCG) evaluation was performed to determine the potential crack growth for the inside surface, outside surface, and embedded flaws in a repaired penetration nozzle. It was determined that the FCG results for the outside surface flaws envelop those for the inside surface flaws and embedded flaws of comparable flaw sizes. Therefore, the FCG results for outside surface flaws are conservatively applied to the inside surface flaws as well as the embedded flaws.

Allowable Axial Flaw Sizes

Figures 2-5 and 2-6 show the fatigue crack growth prediction of the penetration nozzles for a range of flaw depths at the uphill side and downhill side, respectively. It should be noted that the total flaw depth is limited to 75% of the wall thickness in all cases except for the flaws with an aspect ratio (flaw length/flaw depth) of 10. The allowable flaw depth for a flaw with an aspect ratio of 10 is slightly over 74% of the wall thickness as shown in Figure 2-3. The maximum allowable flaw sizes accounting for fatigue crack growth in a repaired penetration nozzle can be determined from these figures by subtracting the fatigue crack growth increments shown on Figures 2-5 and 2-6 from the ASME Code allowable flaw sizes shown on Figure 2-3, for the desired period of service life. Figure 2-7 shows the maximum allowable axial flaw sizes taking into account of fatigue crack growth for a 20 year period of service life.

Allowable Circumferential Flaw Sizes

Figures 2-8 and 2-9 show the fatigue crack growth prediction of the penetration nozzles for a range of flaw depths at the uphill side and downhill side, respectively. It should be noted that the total flaw depth is limited to 75% of the wall thickness in all cases. The maximum allowable flaw sizes accounting for fatigue crack growth in a repaired penetration nozzle can be determined from these figures by subtracting the fatigue crack growth increments shown on Figures 2-8 and 2-9 from the ASME Code allowable flaw sizes shown on Figure 2-4, for the desired period of service life. Figure 2-10 shows the maximum allowable circumferential flaw sizes taking into account of fatigue crack growth for a 20 year period of service life.

2.4 SUMMARY

Axial and circumferential flaws found on the inside surface or outside surface of a head penetration nozzle can be repaired using the embedded flaw repair method to seal it from the primary water environment. The maximum allowable axial and circumferential flaw sizes detected in the penetration nozzles that can be repaired using the embedded flaw repair method are shown in Figures 2-7 and 2-10 with the effects of fatigue crack growth included for a 20 year period of service life. For other periods of service life, the maximum allowable flaw sizes can be determined directly from Figures 2-5, 2-6, 2-8 and 2-9.

Table 2-1 (See also next page)

Summary of Reactor Vessel Transients for Byron and Braidwood Units 1 and 2 [7]

Normal Conditions	Number of Occurrences
Plant Heatup And Cooldown	200 (each)
Plant Loading and Unloading at 15% of Full Power / Minute	13,200 (each)
Step Load Increase and Decrease of 10% of Full Power	2,000 (each)
Large Step Load Decrease with Steam Dump	200
Steady State Fluctuation	infinite
Feedwater Cycling at Hot Shutdown	2,000
Loop Out of Service, Normal Loop Shutdown	80
Loop Out of Service, Normal Loop Startup	70
Unit Loading and Unloading between 0 and 15% Full Power	500 (each)
Boron Concentration Equalization	26,400
Refueling	80
Upset Conditions	
Loss of Load	80
Loss of Power	40
Partial Loss of Flow	80
Reactor Trip From Full Power	400
Inadvertent RCS Depressurization	20
Inadvertent Startup of an Inactive Loop	10
Control Rod Drop	80
Inadvertent S.I. Actuation	60
Test Conditions	
Turbine Roll Test	20
Primary Side Hydrostatic Test	10
Secondary Side Hydrostatic Test	10
Primary Side Leak Test	200
Secondary Side Lead Test	80
Tube Leakage Test	800
Emergency and Faulted Conditions	
Small Loss-of-Coolant Accident (LOCA)	5
Small Steam Break	5

Table 2-1 (Continued)

Summary of Reactor Vessel Transients for Byron and Braidwood Units 1 and 2 [7]

Emergency and Faulted Conditions (Continued)	
Complete Loss of Flow	5
Reactor Coolant Pipe Break (Large LOCA)	1
Large Steam Line Break	1
Feedwater Line Break	1
Reactor Coolant Pump Locked Rotor	1
Control Rod Ejection	1

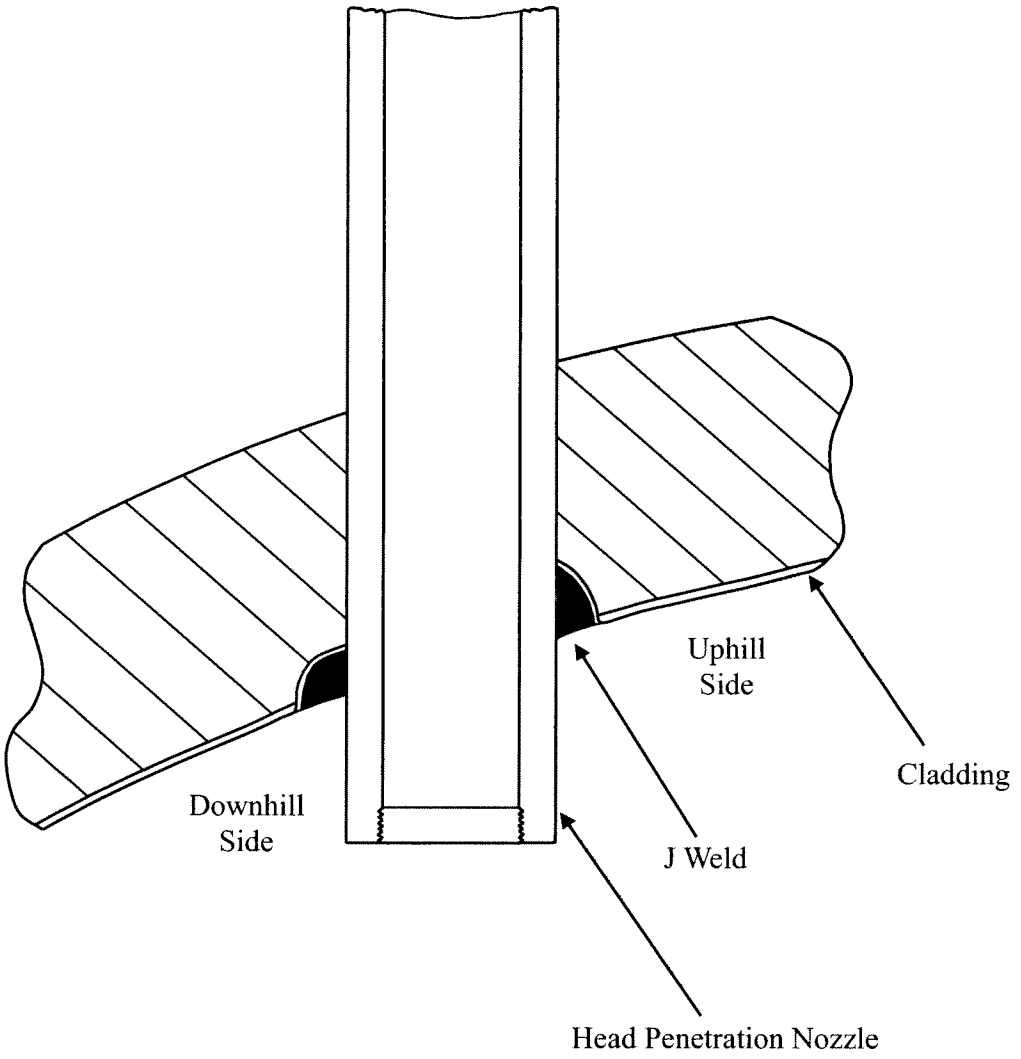

Figure 2-1 Geometry of a Typical Closure Head Penetration

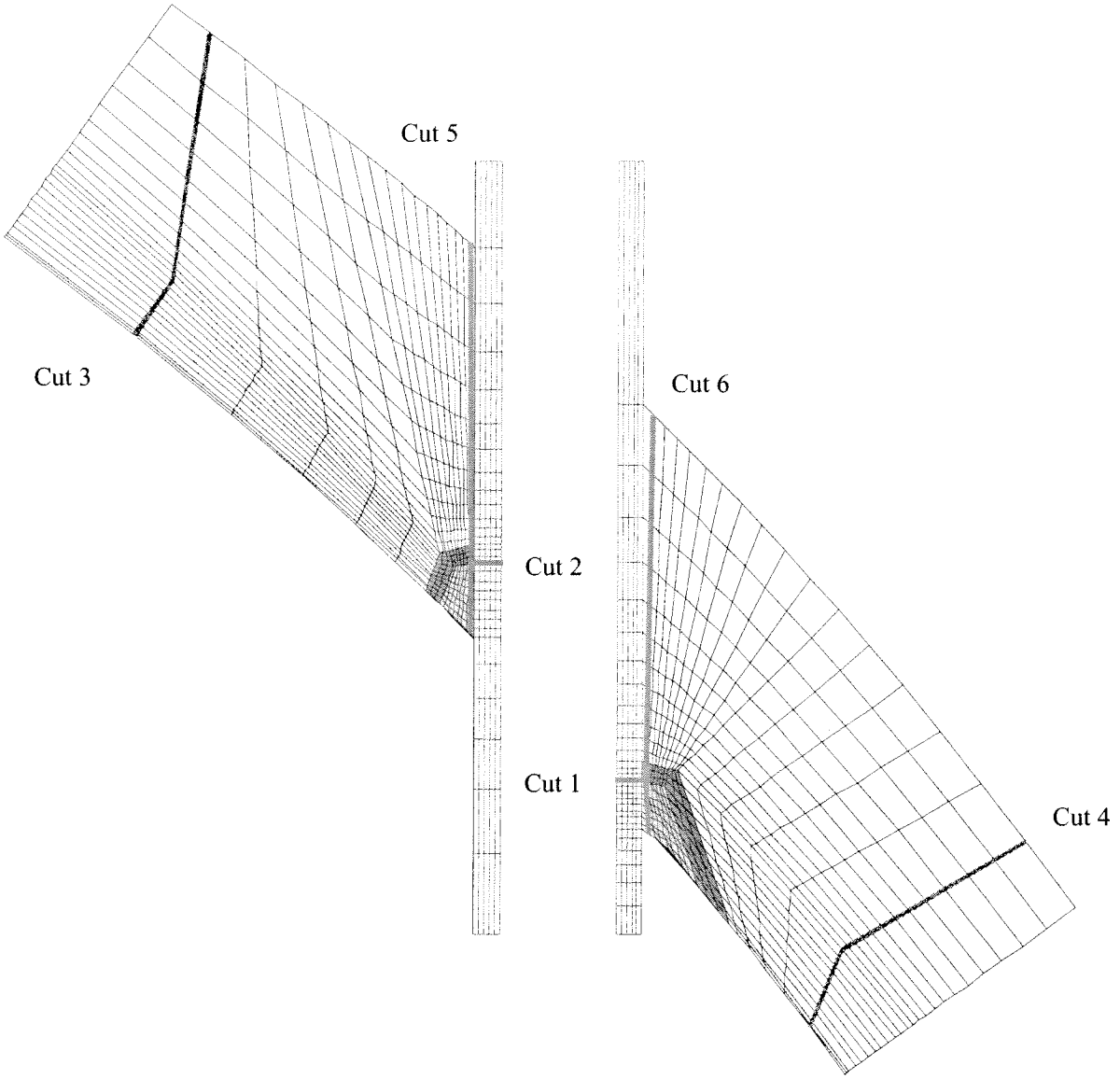

Figure 2-2 Analytical Stress Cuts Taken from the Finite Element Model

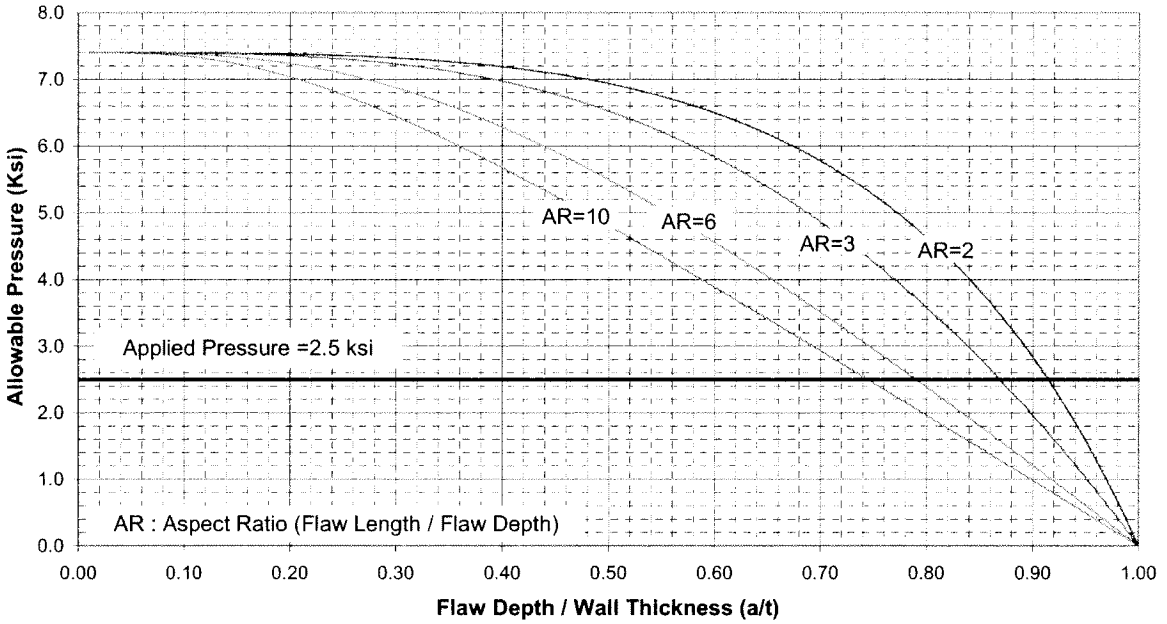

Figure 2-3 Allowable Axial Flaw Sizes In Penetration Nozzle (Without Fatigue Crack Growth)
[ ]^{a,c,e}

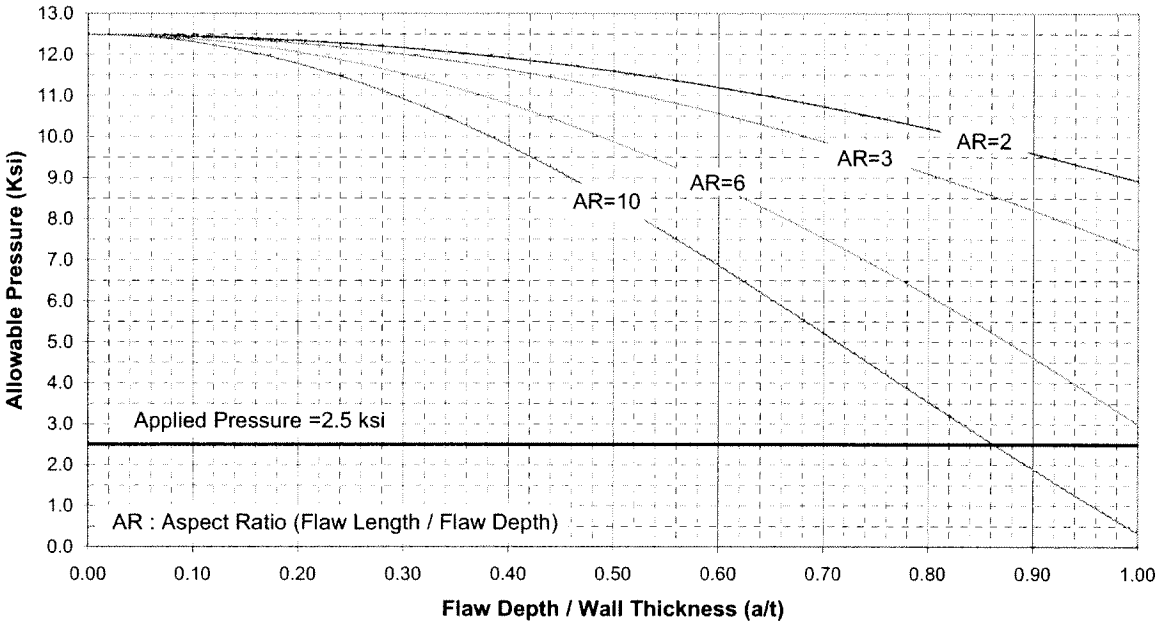

Figure 2-4 Allowable Circumferential Flaw Sizes In Penetration Nozzle (Without Fatigue Crack Growth) [ ]^{a,c,e}

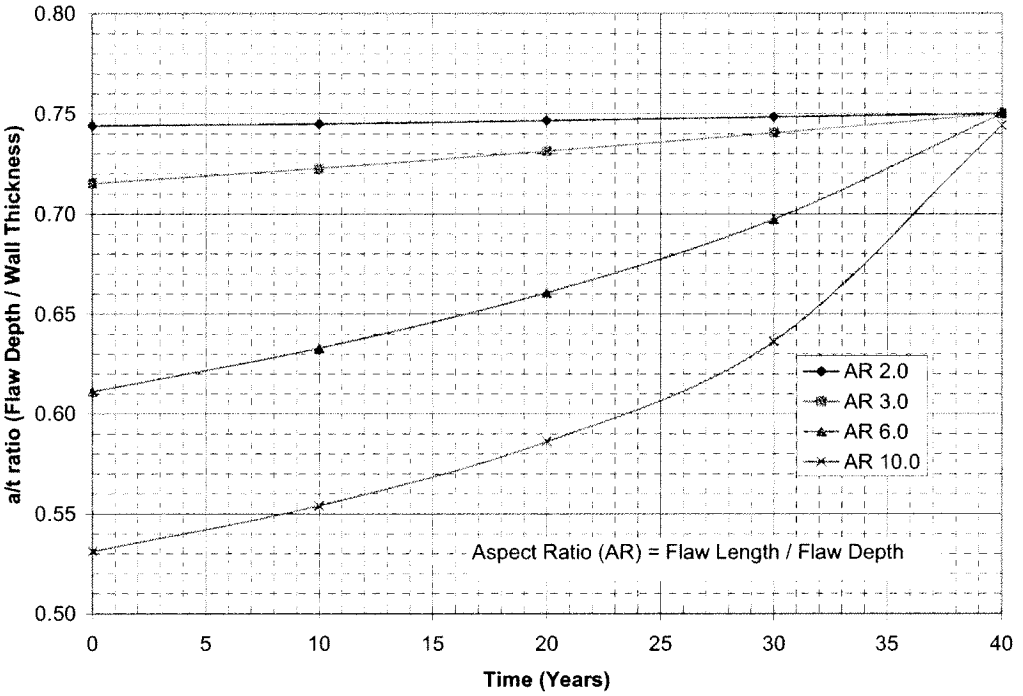

Figure 2-5 Fatigue Crack Growth Prediction for Repaired Axial Flaws in the Penetration Nozzles (Uphill side)

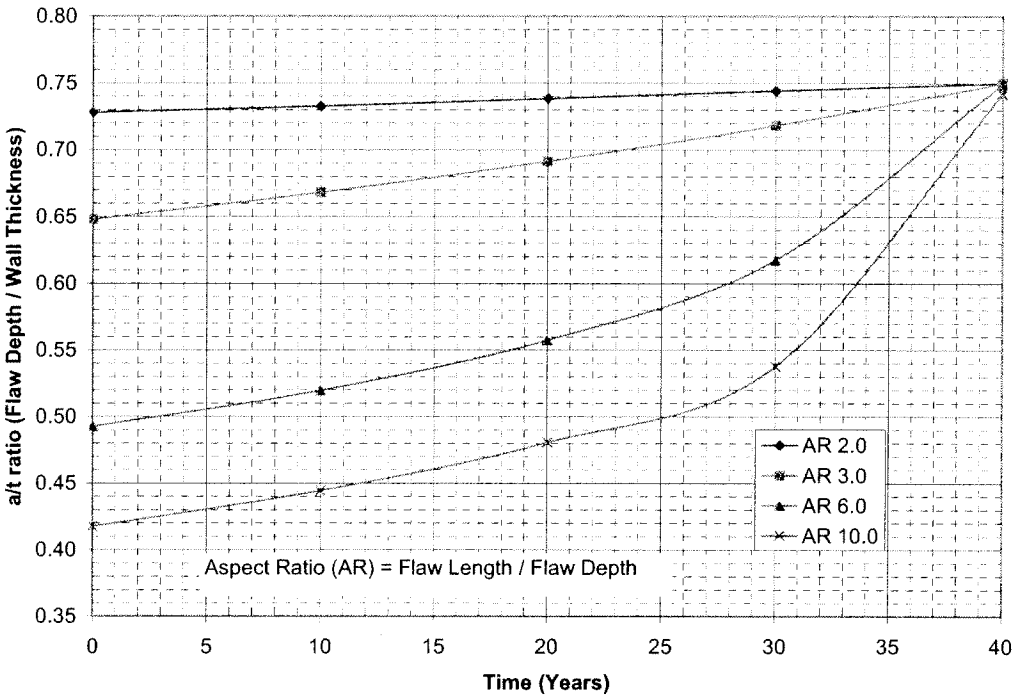

Figure 2-6 Fatigue Crack Growth Prediction for Repaired Axial Flaws in the Penetration Nozzles (Downhill side)

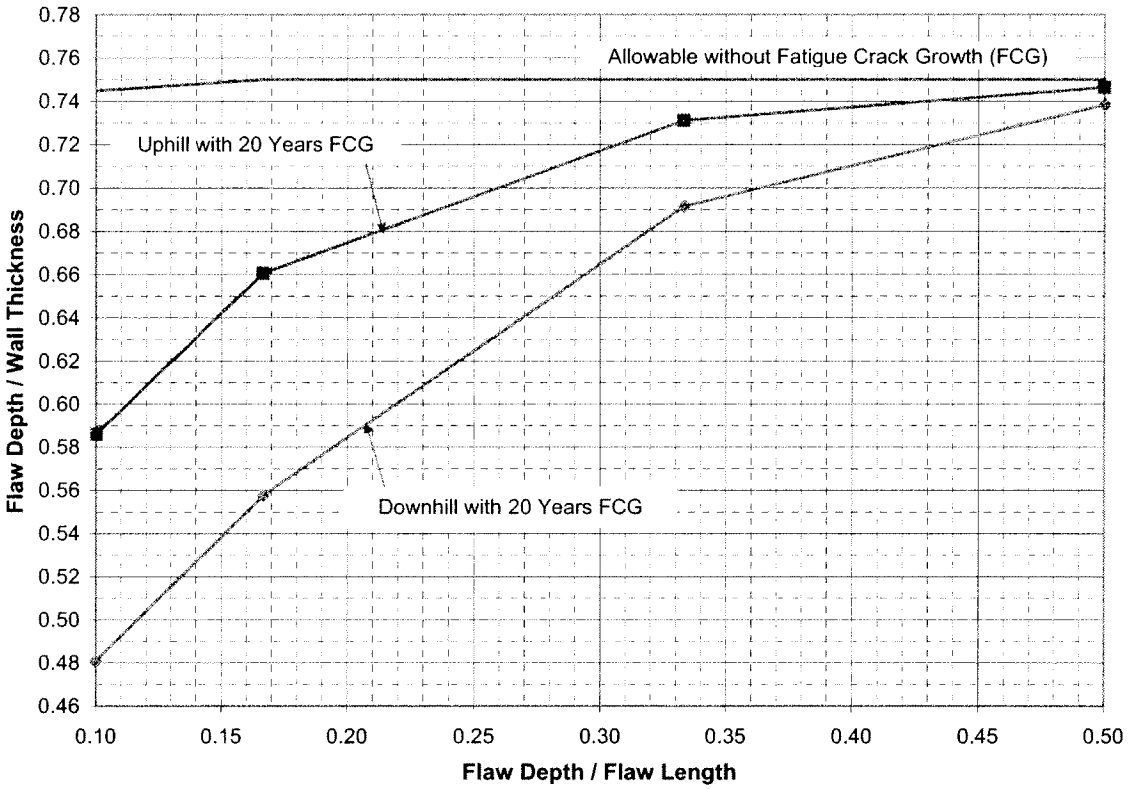

Figure 2-7 Maximum Allowable Axial Flaw Sizes in the Repaired Penetration Nozzles for 20 Years Service Life

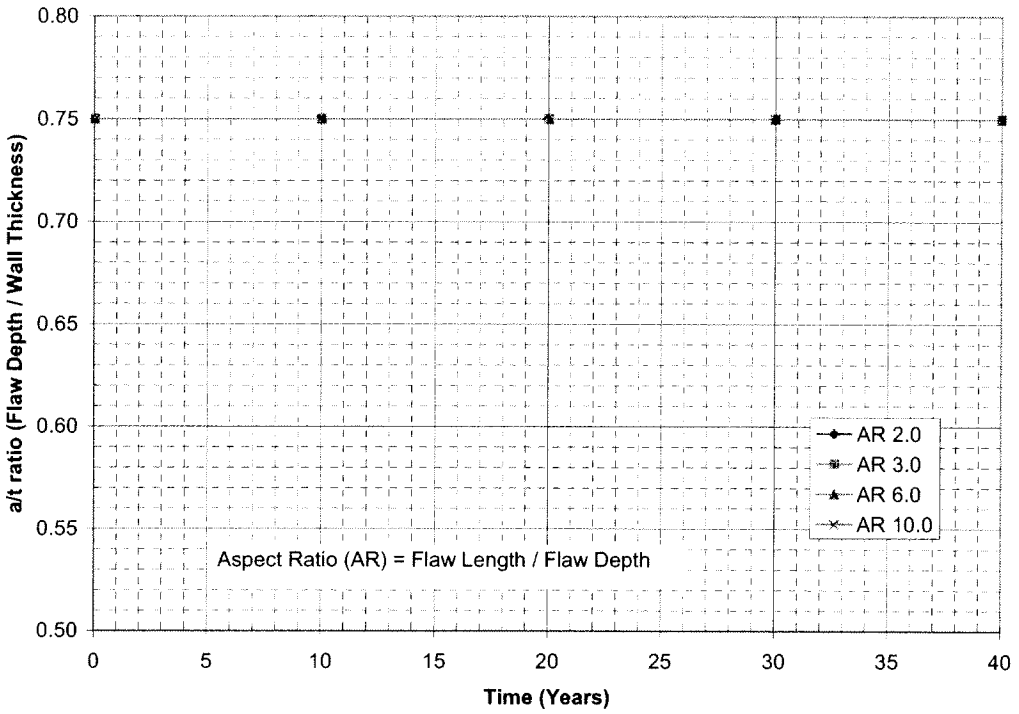

Figure 2-8 Fatigue Crack Growth Prediction for Repaired Circumferential Flaws in the Penetration Nozzles (Uphill side)

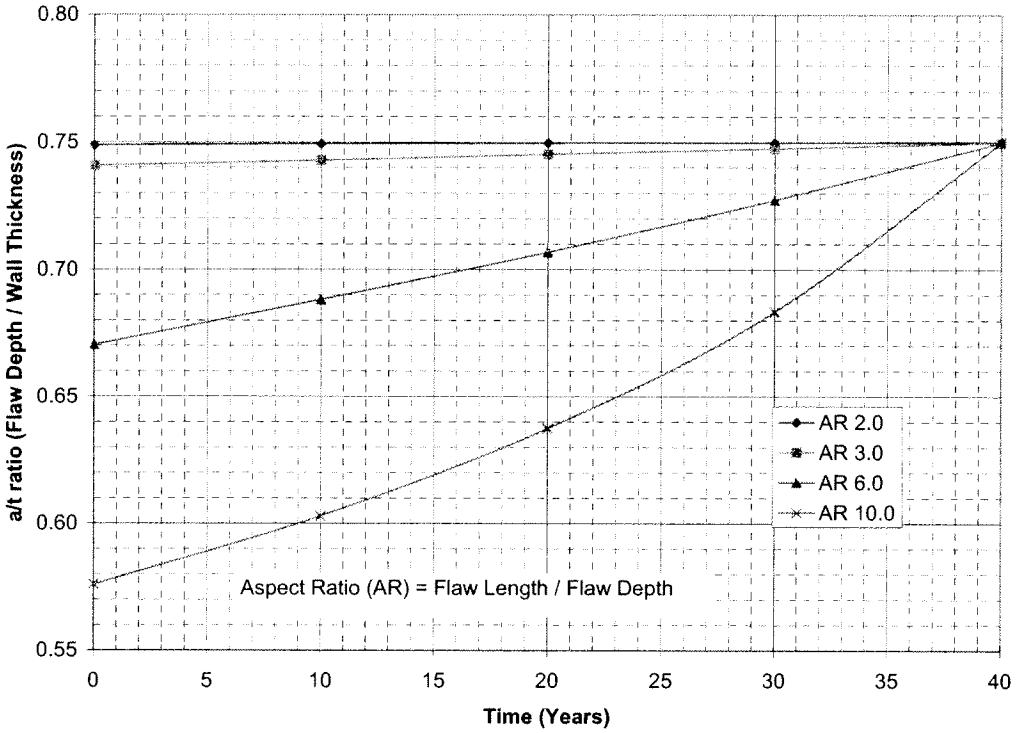

Figure 2-9 Fatigue Crack Growth Prediction for Repaired Circumferential Flaws in the Penetration Nozzles (Downhill side)

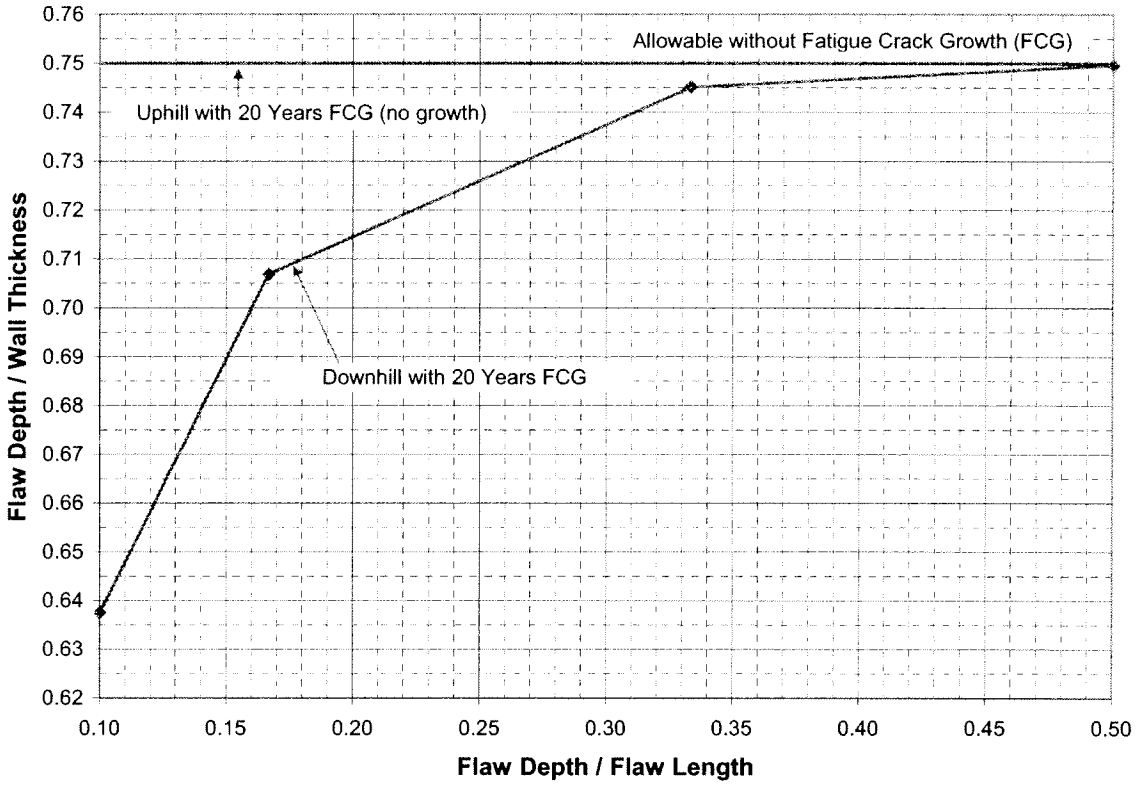

Figure 2-10 Maximum Allowable Circumferential Flaw Sizes in the Repaired Penetration Nozzles for 20 Years Service Life

3 TECHNICAL BASIS FOR APPLICATION OF EMBEDDED FLAW REPAIR METHOD TO PENETRATION NOZZLE ATTACHMENT WELDS

This section provides a discussion on the technical basis for the use of embedded flaw repair method for a flawed head penetration attachment weld. [

]^{a,c,e}

A flaw evaluation was carried out by postulating a planar flaw of that size in the reactor vessel head. Based on the results of the evaluation, the largest flaw size that can be repaired using the embedded flaw repair method was determined.

3.1 Acceptance Criteria

3.1.1 Section XI Appendix K

The acceptance criteria and evaluation procedures used to demonstrate structural integrity of the reactor vessel closure head is contained in Appendix K of ASME Code Section XI [2]. Although the original purpose of Appendix K was to evaluate reactor vessels with low upper shelf fracture toughness, the methods are equally applicable to any region of the reactor vessel where the fracture toughness can be described with elastic plastic parameters. The head region of the reactor vessel is one of the hottest portion of the reactor vessel where the typical steady state temperature is approximately 550-620 °F. This ensures ductile behavior, and so the use of elastic-plastic methods is appropriate.

The approach to evaluating the integrity of a nuclear vessel has been developed over a ten-year period, and has been illustrated with a number of example problems [8] to demonstrate its use. The extension of this methodology to issues other than the low shelf fracture toughness issue is appropriate when service conditions (temperature) ensure ductile behavior. The extension of the Elastic Plastic Fracture Mechanics (EPFM) method to the reactor vessel head is appropriate, as discussed above.

The acceptance criteria are to be satisfied for each category of transients, namely, Service Load Level A (normal), Level B (upset), Level C (emergency) and Level D (faulted) conditions. The criteria are listed below:

$$J < J_{0.1}$$

$$\frac{\partial J}{\partial a} < \frac{dJ_R}{da}$$

J_R = J-integral resistance to ductile tearing for the material

J = Applied J-integral, with a safety factor of 1.15

$J_{0.1}$ = J-integral resistance at a ductile flaw extension of 0.1 inch

$\frac{\partial J}{\partial a}$ = Partial derivative of the applied J-integral with respect to flaw depth, a

$\frac{dJ_R}{da}$ = Slope of the J-R curve

3.1.2 Primary Stress Limits

In addition to satisfying the Section XI criteria, the primary stress limits of paragraph NB-3000 in Section III of the ASME Code must be satisfied. The effects of a local area reduction that is equivalent to the area of the postulated flaw in the vessel head attachment weld must be considered by increasing the membrane stresses to reflect the reduced cross section. The allowable flaw depth was determined by evaluating the primary stress of a spherical head with reduced wall thickness, using design pressure loading of 2500 psia. The results show that the allowable flaw depth is bigger than all the attachment weld sizes.

3.2 METHODOLOGY

The evaluation assumed that a flaw has been detected in a penetration nozzle attachment weld and that the embedded flaw repair method is used to seal the flaw from further exposure to the primary water environment. The evaluation was performed to demonstrate that for a postulated flaw that encompassed the entire attachment weld region in the vessel head near the penetration nozzle, the flaw is stable under ductile crack growth based on the acceptance criteria described in Section 3.1. [ ]^{a,c,e} Therefore, fatigue crack growth evaluations for the postulated flaw in the reactor vessel head and the repair weld were performed to ensure structural integrity.

3.2.1 Geometry and Source of Data

There are many head penetrations in the reactor vessel upper head, and the highest stressed region of the vessel head is chosen for analysis. The distribution of residual, transient thermal, and pressure stresses in the closure head region is obtained from detailed three-dimensional elastic-plastic finite element analyses of the head penetration nozzle region [3] for Byron and Braidwood Units 1 and 2. The outermost penetration nozzle attachment weld regions were chosen for analysis because the stresses are in general highest there. The through-wall stress distributions from the finite element analyses were used to determine the fatigue crack growth and the resulting allowable flaw size for the postulated flaws in the attachment weld regions of the vessel head. The stress cuts on the reactor vessel head were selected for the analysis and the finite element model with the selected stress cuts is shown in Figure 2-2.

3.2.2 Loading Conditions

Thermal Transient Selection for Maximum Allowable Flaw Size Determination

The requirement for an evaluation of a flaw using the rules of Section XI is that the governing transients be chosen for the normal/upset conditions as well as the emergency/faulted conditions. [

]^{a,c,e}

Thermal Transient Selection for Fatigue Crack Growth Prediction

[

]^{a,c,e} The thermal transients that occur in the upper head region are relatively mild because most of the water in the head region has already passed through the core region. The flow in the upper head region is low compared to other regions of the reactor vessel, which mutes the effects of the operating thermal transients. The thermal transients that occur in Byron and Braidwood Units 1 and 2 are shown in Table 2-1. [

]^{a,c,e}

3.2.3 Stress Intensity Factor

One of the key elements in a fracture mechanics evaluation is the determination of the crack driving force or stress intensity factor (K_I). This is based on the information available in the literature.

The stress intensity factors for two corner flaws emanating from the edge of a hole in a plate was taken from the data by [ ]^{a,c,e} Use of this method requires that the stresses remote from the hole be resolved into membrane and bending stress components. The stress intensity factor can be expressed conservatively in terms of the membrane and bending stress components as follows:

[

]^{a,c,e} This flexibility is necessary because this expression will be applied to a range of flaw shapes corresponding to different attachment

weld shapes in Byron and Braidwood Units 1 and 2. The coefficients A and B can be found in [9] for selected values of r/t, a/ℓ and a/t, where "r" is the outside radius of the penetration nozzle and "t" is the wall thickness of the reactor vessel head. For the r/t, a/ℓ and a/t values that are not shown in [9], the coefficients A and B were determined using interpolation. Since the coefficients are provided for various locations around the flaw front, [

]^{a,c,e}

The stress intensity factors for the resulting embedded flaws due to the embedded flaw repair method were calculated based on the method given in Appendix A of Section XI. The sub-surface stress intensity factor expression can be applied to a crack approaching the surface of a component as stated in the technical basis [10]. The stress intensity factor can be expressed in terms of the equivalent membrane and bending stress components as follows:

$$K_I = \left(\sigma_m M_m + \sigma_b M_b\right)\sqrt{\pi a / Q}$$

where

σ_m, σ_b = Equivalent membrane and bending stresses, as defined in A-3200(a) of the Code [2]. (See Figure 3-4)

M_m, M_b = Correction factors for the membrane and bending stresses. The equations for the correction factors are listed in [10]

a = One-half the axis of elliptical flaw

Q = Flaw shape parameter as defined in [10]

3.2.4 Material Properties

One of the most important information on the toughness for pressure vessel and piping materials is the J-R curve of the material, where J-R stands for material resistance to crack extension, as represented by the measured J-integral value versus crack extension. Simply put, J-R curve to cracking resistance is as significant as the stress-strain curve to load-carrying capacity and ductility of a material. Both J-R curve and stress-strain curve are properties of a material.

Unfortunately, directly measured J-R curves are not generally available for a specific material of interest. Fortunately, methods that can generate such information from available data such as material chemistry, radiation exposure, temperature and Charpy V-notch energy, is now available [11]. The method provided in [11] summarizes a large collection of public test data, and fitted into multivariable model based on advanced pattern recognition technology. Separate analysis models and databases were developed for different material groups, including reactor pressure vessel (RPV) welds, RPV base metals, piping welds, piping base metals and a combined materials group.

The material resistance J-values, J_{mat}, are fitted into the following equation [11, 12]:

$$J_{mat} = (MF)C1\,(\Delta a)^{C2} \exp\left[C3(\Delta a)^{C4}\right]$$

where C1, C2, C3, and C4 are fitting constants, and Δa is crack extension

MF is the Margin Factor from [12]:
MF= 0.749 for Service Levels A, B and C
MF= 1.0 for Service Level D

For the RPV base metal model, the constants C1, C2, C3, and C4 are taken from Table 11 of [11]. C1, C2, C3, and C4 are complicated parameters as defined below:

$$\ln C1 = a_1 + a_2 \ln CVNp + a_3 T + a_4 \ln B_n + a_5 \phi t$$
$$C2 = d_1 + d_2 \ln C1 + d_3 \ln B_n$$
$$C3 = d_4 + d_5 \ln C1 + d_6 \ln B_n$$
$$C4 = d_7$$

where T = Temperature (°F),
B_n = Section thickness (inches).
CVNp = Charpy impact energy (ft-lbs) = 114 ft-lb from [13].
ϕt = Fluence ($x10^{18}$ n/cm^2, E>1Mev).

a_1, a_2, a_3, a_4, a_5, d_1, d_2, d_3, d_4, d_5, d_6, d_7 (briefly, a_i and d_i) are constants given in Table 11 of [11]:

a1 = -2.44
a2 = 1.13
a3 = -0.00277
a4 = 0.0801
d1 = 0.0770
d2 = 0.116
d3 = -0.0412
d4 = -0.0812
d5 = -0.00920
d6 = -0.0295
d7 = -0.409

Neutron irradiation has been shown to produce embrittlement that reduces the toughness properties of reactor vessel ferritic steel material. The irradiation levels are very low in the reactor vessel head region and therefore the fracture toughness will not be measurably affected.

3.2.5 Applied J-Integral

For small scale yielding, $J_{applied}$ of a crack can be calculated by the Linear Elastic Fracture Mechanics (LEFM) method. A plastic zone correction must be performed to account for the plastic deformation at the crack tip. The plastic deformation ahead of the crack front is then regarded as a failed zone and the crack size is, in effect, increased. The K_I-values can be converted to $J_{applied}$ by the following equation:

$$J_{applied} = \frac{K_{ep}^2}{E'}$$

where K_{ep} is the elastically calculated K_I-value based on the plastic zone adjusted crack depth or size

$E' = E/(1-\nu^2)$ for plane strain, $E' = E$ for plane stress, E = Young's Modulus,
and ν = Poisson's Ratio.

The plastic zone size, r_p, is calculated by

$$r_p = \frac{1}{6\pi}\left(\frac{K_I}{S_y}\right)^2$$

where S_y is the yield strength of the material. Assume that the crack depth is a_o, the K_{ep} can now be calculated based on a new crack length, $a_o + r_p$. For small scale yielding, K_{ep} can be simplified as follows:

$$K_{ep} = f\ K_I$$

Where $f = \sqrt{\frac{(a_0 + r_P)}{a_0}}$

3.2.6 Fatigue Crack Growth Prediction

The analysis procedure involves postulating planar flaws that extend radially over the entire attachment weld cross-section in the vessel head and are subjected to a series of design loads. The loading included pressure, thermal transients, and residual stresses. The transients used for this evaluation are shown in Section 3.2.2 and the cycles are distributed evenly over the plant design life. The stress intensity factor range, ΔK_I, which controls the fatigue crack growth, depends on the geometry of the crack, its surrounding structure and the range of applied stresses in the region of the postulated crack. Once ΔK_I is calculated, the fatigue crack growth due to a particular stress cycle can be determined using a crack growth rate reference curve applicable to the material where the crack is postulated.

The crack growth rate (CGR) curves used in the analyses for the postulated flaws in the reactor vessel head are taken directly from Appendix A in the 2004 Edition of ASME Code Section XI for ferritic steels. Since the flaw is sealed from the primary water environment, the crack growth rate reference curve for the air environment is used. This curve is a function of the applied stress intensity factor range (ΔK_I) and the R ratio, which is the ratio of the minimum to maximum stress intensity factor during a thermal transient. The crack growth equation is given below:

$$\frac{da}{dN} = C_o(\Delta K - K_{th})^{3.07}$$

where:

$\frac{da}{dN}$ = Crack growth rate, inches/cycle

ΔK_I = Stress intensity factor range, ksi $\sqrt{in}$
= $(K_{Imax} - K_{Imin})$

ΔK_{th} = ΔK_I threshold value, ksi $\sqrt{in}$
= 5.0 (1 - 8.0 R) for $0 \leq R < 1.0$

$$C_o = 1.99 \times 10^{-10} S$$

$$S = 25.72 (2.88 - R)^{-3.07} \text{ for } 0 \leq R < 1.0$$

$$R = K_{I\,min} / K_{I\,max}$$

The crack growth rate reference curve in air used in determining the fatigue crack growth into the repair weld Alloy 52 is not available. However, there are limited test data on Alloy 52 in PWR water environment and, based on these data, the crack growth rates for Alloy 52 and Alloy 600 were concluded to be the same in PWR water environment [6]. Therefore, the crack growth rate curve for Alloy 52 in air is assumed to be the same as that for Alloy 600 in air, which is shown in Equation 2-7 of Section 2.

Once the incremental crack growth corresponding to a specific transient for a small time period is calculated, it is added to the original crack size and the analysis continues to the next time period and/or thermal transient. The procedure is repeated in this manner until all the significant analytical thermal transients and cycles known to occur in a given period of operation have been analyzed.

3.3 FRACTURE MECHANICS ANALYSIS RESULTS

3.3.1 Results for Applied J-Integral and Material J-R Curves

The actual geometry or weld shapes of Byron and Braidwood Units 1 and 2 head penetration attachment welds [14] are shown in Table 3-1 and Figure 3-1, which forms the basis for the geometry of the postulated flaws in the attachment weld region. The stress intensity factors were calculated for the worst attachment weld shapes (lowest a/ℓ ratio), which are the downhill side welds for the outermost penetration No. 74-78. These attachment weld shapes with the lowest a/ℓ ratio were selected to bound all the other penetration nozzle attachment weld shapes in both Byron and Braidwood Units 1 and 2.

The applied J-integral values for the worst attachment weld shapes were calculated based on the method described in Section 3.2.5. The material J-R Curve was obtained as discussed in Section 3.2.4 by setting the Margin Factor (MF) to 0.749. The applied J-integral values and the material J-R Curve were tabulated in Table 3-2 and plotted in Figure 3-2. Using the acceptance criteria shown in Section 3.1, the structural integrity of the reactor vessel head with a postulated flaw that encompassed the entire attachment weld region can then be determined.

The key aspects of the structural integrity evaluation are the values of the applied J-integral versus that for the reactor vessel head material and the slope of the J-applied curve versus the slope of the material J-R curve. Figure 3-2 demonstrated the structural stability of a postulated flaw with the worst attachment weld shape. In Figure 3-2, it can be seen that for a crack extension of 0.1 inch with an initial flaw depth of 1.55 inch, the applied J-integral value is below that of the material J-R curve. In addition, the slope of the material J-R curve exceeds that of the J-applied curve. Since the acceptance criteria in Section 3.1 is met for the worst attachment weld shape, it can be concluded that structural stability is also demonstrated for all postulated flaws with the attachment weld shapes tabulated in Table 3-1.

3.3.2 Results for Fatigue Crack Growth into the Vessel Head

Fatigue crack growth was determined for postulated flaws in the reactor vessel head with attachment weld shapes on the uphill and downhill sides of the penetration nozzles that envelop all the other attachment weld shapes in both Byron and Braidwood Units 1 and 2. As shown in Figure 3-3, the predicted crack growth for the uphill side is slightly higher than that for the downhill side, but in general, the fatigue crack growth is quite small. Based on the fatigue crack growth results, stability of postulated flaws which encompassed the entire attachment region can be shown stable for at least 10 years of service life.

3.3.3 Results for Fatigue Crack Growth into the Repair Weld

[

]^{a,c,e} The fatigue crack growth result indicates that the repaired weld can last at least 10 years of service life based on the conservatively assumed initial flaw depth.

3.4 SUMMARY

The results of the evaluation have demonstrated that the embedded flaw repair method is a viable method for repairing flaws found in the J-weld. The repair weld layer would last at least 10 years of service life regardless of the size of the flaw found in the penetration nozzle attachment weld. In addition, structural stability can also be demonstrated for at least 10 years of fatigue crack growth regardless of the size of the flaw found in the penetration nozzle attachment weld.

Table 3-1

Geometry of Byron and Braidwood Units 1 and 2
Head Penetration Attachment Welds (All dimensions in inches)

	Uphill				Downhill		
Pen. No.	ℓ	a	a/ℓ		ℓ	a	a/ℓ
1	1.61	1.86	1.155		1.61	1.86	1.155
2-5	1.56	1.98	1.269		1.73	1.75	1.012
6-9	1.56	2.03	1.301		1.81	1.70	0.939
10-13	1.56	2.05	1.314		1.85	1.68	0.908
14-17	1.58	2.11	1.335		1.98	1.62	0.818
18-21	1.59	2.13	1.340		2.02	1.61	0.797
22-29	1.59	2.15	1.352		2.07	1.59	0.768
30-37	1.62	2.21	1.364		2.22	1.55	0.698
38-41	1.66	2.26	1.361		2.40	1.50	0.625
42-49	1.67	2.28	1.365		2.46	1.49	0.606
50-53	1.69	2.30	1.361		2.53	1.47	0.581
54-61	1.72	2.34	1.360		2.68	1.44	0.537
62-65	1.80	2.44	1.356		3.45	1.65	0.478
66-73	1.83	2.46	1.344		3.60	1.63	0.453
74-78	1.89	2.54	1.344		4.11	1.55	0.377

Note : The values a (weld depth) and ℓ (weld length) are dimensions of the J-groove weld only and do not include the dimensions of the fillet weld

Table 3-2 Results of Applied J-integral and Material J-R Curve

a (inch)	J_{mat} (kip-in/in^2)	$J_{applied}$ (kip-in/in^2)
1.550	0.5639	1.4697
1.554	0.6794	1.4735
1.558	0.7724	1.4773
1.562	0.8507	1.4811
1.566	0.9184	1.4849
1.570	0.9783	1.4887
1.574	1.0320	1.4925
1.578	1.0807	1.4963
1.582	1.1254	1.5000
1.586	1.1667	1.5038
1.590	1.2051	1.5076
1.594	1.2410	1.5114
1.598	1.2747	1.5152
1.602	1.3065	1.5190
1.606	1.3367	1.5228
1.610	1.3653	1.5266
1.614	1.3925	1.5304
1.618	1.4185	1.5342
1.622	1.4434	1.5380
1.626	1.4673	1.5418
1.630	1.4902	1.5456
1.634	1.5123	1.5493
1.638	1.5336	1.5531
1.642	1.5542	1.5569
1.646	1.5740	1.5607
1.650	1.5933	1.5645
1.654	1.6119	1.5683
1.658	1.6300	1.5721
1.662	1.6476	1.5759
1.666	1.6646	1.5797
1.670	1.6812	1.5835
1.674	1.6974	1.5873
1.678	1.7131	1.5911
1.682	1.7285	1.5949
1.686	1.7435	1.5987
1.690	1.7581	1.6024
1.694	1.7724	1.6062
1.698	1.7864	1.6100
1.702	1.8001	1.6138
1.706	1.8135	1.6176

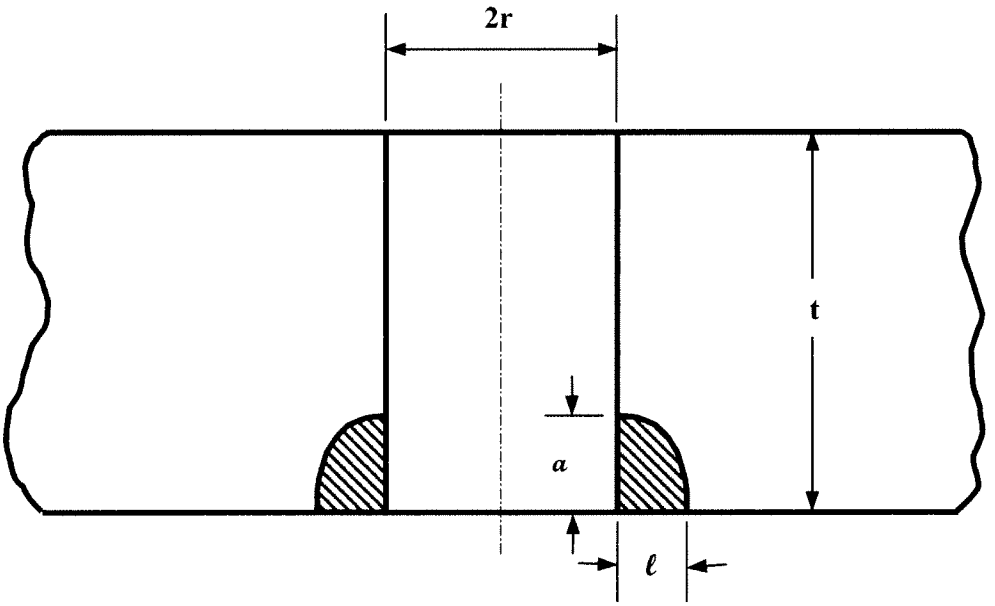

Figure 3-1 Geometry and Terminology as Applied in [ ]^{a,c,e}

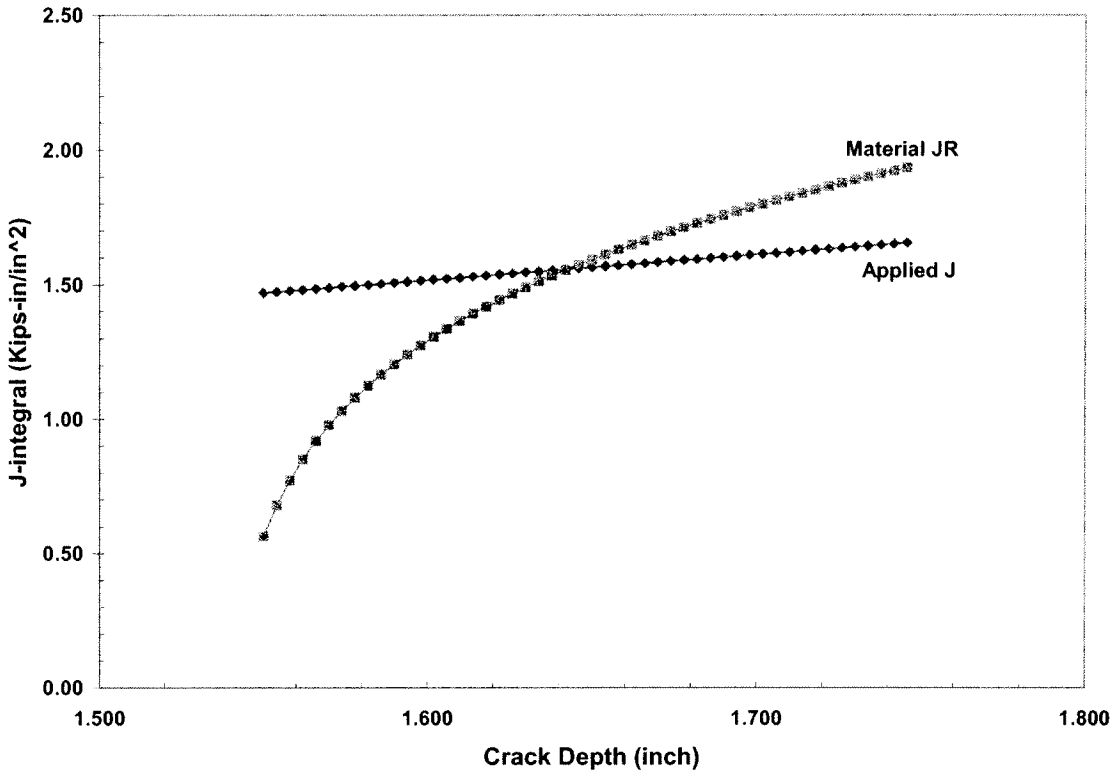

Figure 3-2 Comparison of the Slope of the Applied J-integral and Material J-R Curve (Governing Transient: Loss of Load)

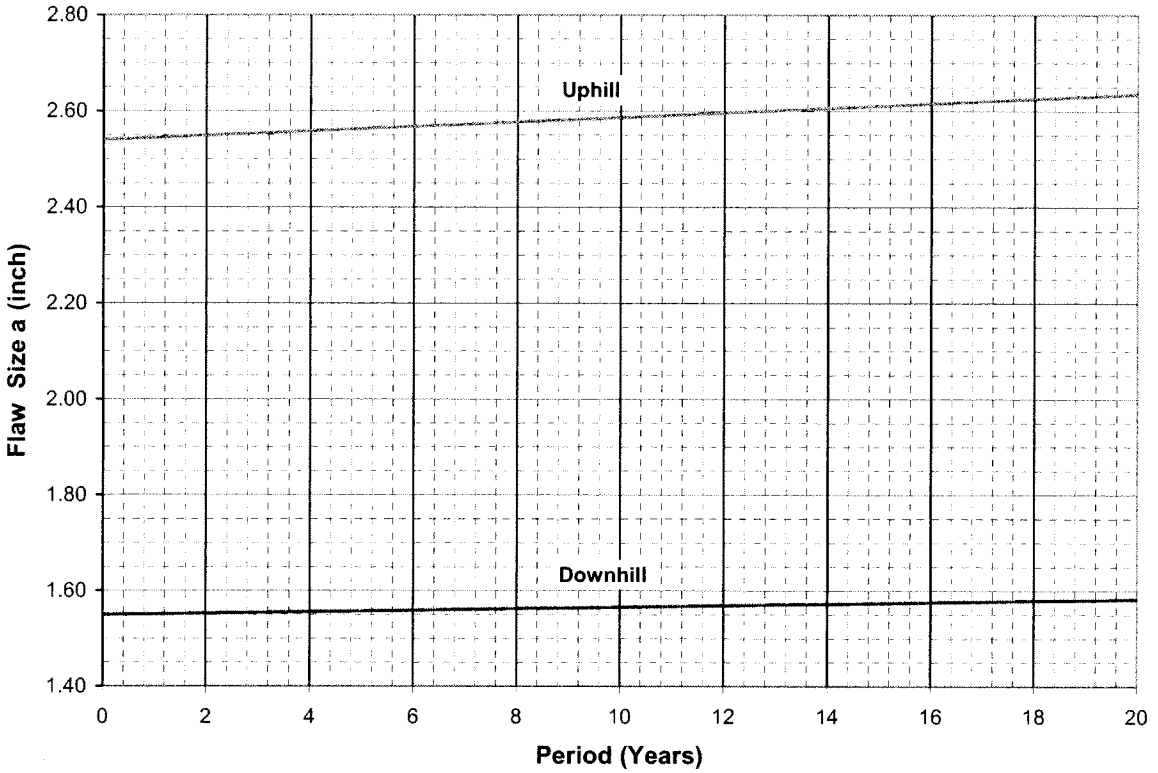

Figure 3-3 Fatigue Crack Growth Prediction in the Reactor Vessel Head with Maximum Postulated Flaws in the Attachment Weld

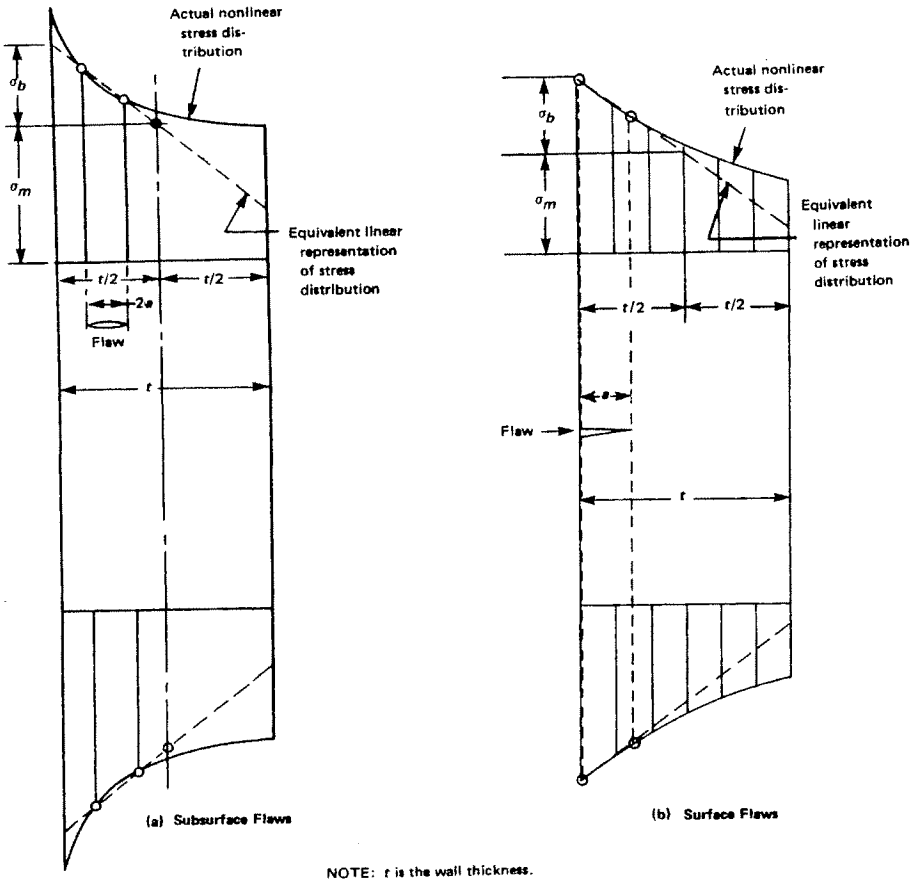

FIG. A-3200-1 LINEARIZED REPRESENTATION OF STRESSES

Figure 3-4 Linearized Representation of Through-Wall Stress Distribution

4 TECHNICAL BASIS FOR "AS-EXCAVATED" REPAIRS

4.1 Introduction

Cracks have been detected on the lower part of the reactor vessel closure head penetration nozzles in some operating plants, both foreign and domestic. Cracks have also been detected in the J-groove attachment welds. The root cause of the problem has been identified as Primary Water Stress Corrosion Cracking (PWSCC) of the Alloy 600 penetration material, or welds.

One of the repair options is to excavate the inside surface of the penetration nozzle on and around each individual crack location. Excavation will serve to remove the material that contains the crack from the penetration nozzle, thus removing the crack.

The purpose of this evaluation is to determine the maximum allowable excavation depth and geometry into the penetration nozzle inside surface, which will still meet the same ASME Code Section III stress allowable that were used in the reactor vessel stress report for Byron and Braidwood Units 1 and 2 [15]. In addition, cyclic stresses induced during normal and upset operating conditions are compared against the ASME code fatigue allowable criteria.

4.2 Technical Approach and Acceptance Criteria

A range of excavation sizes in the penetration nozzles was evaluated to determine the maximum excavation depth. The approach used here is to reconcile the stresses used in the original stress report to account for various excavation depths, and to determine the maximum excavation depth which would still meet the ASME Code Section III requirements used in the Byron and Braidwood Units 1 and 2 reactor vessel stress report [15]. The key dimensions of the head penetration nozzles are shown in Table 4-1. Other key dimensions include the minimum vessel head thickness, which is 6.625 inches, and the inside radius of the spherical head, which is 88.156 inches. The vessel heads and penetration nozzles for both Byron and Braidwood units have the same sizes.

The results presented in this section are based on the original reactor vessel stress qualification report for both Byron and Braidwood Units 1 and 2 [15]. The report provides the technical basis for the original design compliance with the Section III Code requirements. The effects of excavation in the regions of interest will be reflected in higher membrane stresses, and the limiting excavation depths will be those which meet the code stress limits.

The design loads include mechanical, thermal, and other external loads. The effect of other external loads in this region is negligible, because the moments are taken out at the location where the penetration nozzle exits the vessel head. Thus, the effects of the seismic and pipe break loads would be negligible at the location of interest.

The ASME Section III acceptance criteria used in the Byron and Braidwood Units 1 and 2 reactor vessel stress report are shown in Table 4-2. In addition, the local primary stress plus average primary stress was also calculated and shown to satisfy the Section III Code requirements. The loads and material properties used are the same as those used in the original reactor vessel stress report.

Results are provided for the following locations of possible excavation:

1. Penetration nozzles at and above the attachment weld
2. Penetration nozzles below the attachment weld

4.3 Evaluation Results for the "As-Excavated" Repairs

At and Above the Attachment Weld Region

For the penetration nozzle excavation analysis, a 360-degree grind-out was conservatively considered, resulting in a simple thickness reduction in the nozzle. There was no limitation in length. Reducing the nozzle thickness increases the primary stress, and has a small effect on the secondary stress. It was assumed that any grinding performed would have a 3:1 taper or greater in order to minimize any stress concentration effects and any sharp corners or notches resulting from the grinding operations should be eliminated.

For the penetration nozzle, the required minimum wall thickness of the nozzle was calculated to be 0.375 inch. So for a nominal wall thickness of 0.625 inch, the allowable depth of grinding is 0.250 inch. This amounts to a grinding depth of 40 percent of the penetration nozzle nominal wall thickness.

Below the Attachment Weld Region

The region of the penetration nozzles below the attachment weld is not part of the pressure boundary, so there are few restrictions on grinding in this region. Also there are no net pressure loads here, so there are no restrictions on the minimum wall thickness. In an extreme case, the entire penetration nozzle below the weld could be removed. If grinding is performed in this region, care should be taken to ensure that no sharp corners or notches are created and that the potential for loose part is minimized. The slope of the grinding should also maintain a 3:1 taper or greater.

4.4 SUMMARY

Allowable excavation depths have been determined for Byron and Braidwood Units 1 and 2 reactor vessel head penetration nozzles. The approach used here is to reconcile the stresses used in the original stress report to account for various excavation depths, and to determine the maximum excavation depth which would meet the ASME Code Section III requirements.

For excavation on penetration nozzles at or above the attachment region, grinding can be justified to a depth of 40 percent of the nominal wall thickness with a minimum required wall thickness of 0.375 inch. For excavation on penetration nozzles below the attachment weld region, there are no excavation depth limits, as this region is within the pressure boundary. In either case, grinding should have a 3:1 taper or greater in order to minimize any stress concentration effects. Sharp corners or notches resulting from the grinding operations should be eliminated.

Table 4-1 Key Dimensions of Head Penetration Nozzles [14]	
Inside Diameter (in.)	**Outside Diameter (in.)**
2.75	4.00

Table 4-2 Results of Structural Qualification for "As-Excavated" Repairs (Housing Penetration Wall Thickness Reduced to 0.375 inch)			
Category	**Stress Intensity (ksi)**	**Allowable (ksi)**	**Fatigue Usage Factor**
P_L+P_b+Q[a]	< 69.9	3.0 S_m = 69.9	< 1.0 [b]
P_m	20.5	1.5 S_m = 35.0	---
[a] Criterion from [15]			
[b] Allowable Fatigue Usage Factor is 1.0			

5 SUMMARY AND CONCLUSIONS

Engineering evaluations were performed to support the repair efforts associated with the reactor vessel head penetration inspection program for Byron and Braidwood Units 1 and 2.

The technical basis for the use of the embedded flaw repair method if indications or flaws are found in the head penetration nozzle is provided in Section 2. Axial and circumferential flaws found on the inside surface or outside surface of a head penetration nozzle can be repaired using the embedded flaw repair method to seal the flaws from the primary water environment. The maximum allowable axial and circumferential flaw sizes detected in the penetration nozzles that can be repaired using the embedded flaw repair method are shown in Figures 2-7 and 2-10 with the effects of fatigue crack growth included.

The technical basis for the use of the embedded flaw repair method if indications or flaws are found in the head penetration attachment welds is provided in Section 3. The results of the evaluation have demonstrated that the embedded flaw repair method is a viable method for repairing flaws found in the J-weld. The repair weld layer would last at least 10 years of service life regardless of the size of the flaw found in the penetration nozzle attachment weld. In addition, structural stability can also be demonstrated for at least 10 years of fatigue crack growth regardless of the size of the flaw found in the penetration nozzle attachment weld.

The evaluations which address the effects of local structural discontinuities resulting from the grinding operations performed to excavate flaws in the head penetration nozzle are provided in Section 4. For excavation on penetration nozzles at or above the attachment weld region, grinding can be justified to a depth of 40 percent of the nominal wall thickness with a required minimum wall thickness of 0.375 inch. For excavation on penetration nozzles below the attachment weld region, there are no excavation depth limits, as this region is within the pressure boundary. In either case, grinding should have a 3:1 taper or greater in order to minimize any stress concentration effects. Sharp corners or notches resulting from the grinding operations should be eliminated.

Plant specific technical basis for the use of the embedded flaw repair method is presented in this report and it is concluded that Byron and Braidwood Units 1 and Unit 2 meet the criteria for application of the embedded flaw repair process stated in Appendix C of WCAP-15987-P [1].

6 REFERENCES

1. [
]a,c,e

2. ASME Code Section XI, "Rules for Inservice Inspection of Nuclear Plant Components," 2004 Edition.

3. Fleming, M., et al. "CRDM Nozzle Transient Stress Analysis: Byron & Braidwood Reactor Vessel Heads," Dominion Engineering, Inc. Report R-8705-00-1, Revision 0, December 2004.

4. Brown, C. M., and Mills, W. J., "Fracture Toughness, Tensile and Stress Corrosion Cracking Properties of Alloy 600, Alloy 690, and Their Welds in Water," in Proceedings of Corrosion 96, Paper 90.

5. [
]a,c,e

6. NUREG/CR-6721, ANL-01/07, "Effects of Alloy Chemistry, Cold Work, and Water Chemistry on Corrosion Fatigue and Stress Corrosion Cracking of Nickel Alloys and Welds," April 2001.

7. [
]a,c,e

8. "Development of Criteria for Assessment of Reactor Vessels with Low Upper Shelf Fracture Toughness," Welding Research Council Bulletin 413, July 1996.

9. [
]a,c,e

10. Marston, T. U. et al., "Flaw Evaluation Procedures: ASME Section XI," Electric Power Research Institute Report EPRI-NP-719-SR, August 1978.

11. E. D. Eason, J. E. Wright, E. E. Nelson, "Multivariable Modeling of Pressure Vessel and Piping J-R Data," NUREG/CR-5729, MCS 910401, RF, R5, May 1991.

12. Regulatory Guide 1.161, "Evaluation of Reactor Pressure Vessel with Charpy Upper-Shelf Energy Less Than 50 ft-lb".

13. Reference Documents for Charpy Impact Energy for Byron and Braidwood Units 1 and 2.

    a) [
    ]a,c,e

    b) [
    ]a,c,e

c) [

]^{a,c,e}

d) [

]^{a,c,e}

14. Reference Drawings for Byron and Braidwood Units 1 and 2:

a) B&W Drawing No. 184573E, Revision 4, "Closure Head Assembly". (Byron 1)

b) B&W Drawing No. 184574E, Revision 6, "Closure Head Sub-Assy Sheet#1". (Byron 1)

c) B&W Drawing No. 184577E, Revision2, "Control Rod Mech. Housing". (Byron 1)

d) B&W Drawing No. 185282E, Revision 0, "Closure Head Assembly". (Byron 2)

e) B&W Drawing No .185283E, Revision 1, "Closure Head Sub-Assy Sheet#1". (Byron 2)

f) B&W Drawing No. 185286E, Revision 1, "Control Rod Mech. Housing". (Byron 2)

g) B&W Drawing No. 185313E, Revision 0, "Closure Head Assembly". (Braidwood 1)

h) B&W Drawing No. 185314E, Revision 0, "Closure Head Sub-Assy Sheet#1". (Braidwood 1)

i) B&W Drawing No. 185317E, Revision 0, "Control Rod Mech. Housing". (Braidwood 1)

j) B&W Drawing No. 185344E, Revision 0, "Closure Head Assembly". (Braidwood 2)

k) B&W Drawing No. 185345E, Revision 0, "Closure Head Sub-Assy Sheet # 1". (Braidwood 2)

l) B&W Drawing No. 185348E, Revision 0, "Control Rod Mech. Housing". (Braidwood 2)

15. [

]^{a,c,e}